Title: Systematic characterization of brain cellular crosstalk reveals a novel role for SEMA6D in TREM2-associated microglial function in Alzheimer's disease

Authors: Ricardo D'Oliveira Albanus[1,2,3]*, Gina M Finan[4,5]*, Logan Brase[1,2,3], Shuo Chen[6], Qi Guo[7], Abhirami Kannan[1,2,3], Mariana Acquarone[1,2,3], Shih-Feng You[1,2,3], Brenna C Novotny[1,2,3], Patricia M Ribeiro Pereira[8], John C Morris[2,9,10,11], David M Holtzman[2,9,10,11], Eric McDade[1,11], Martin Farlow[11,12], Jasmeer P Chhatwal[11,13], Dominantly Inherited Alzheimer Network (DIAN)[11], Emily E Mace[14], Bruno A Benitez[15], Laura Piccio[2,16,17], Greg T Sutherland[18], Qin Ma[7], Hongjun Fu[6], Celeste M Karch[1,2,3,11], Oscar Harari[1,2,3†], Tae-Wan Kim[4,5†]

[1] Department of Psychiatry, Washington University School of Medicine, St. Louis, MO, USA
[2] Hope Center for Neurological Disorders, Washington University School of Medicine, St. Louis, MO, USA
[3] NeuroGenomics and Informatics, Department of Psychiatry Washington University in St. Louis
[4] Department of Pathology and Cell Biology, Columbia University Irving Medical Center, New York, NY, USA
[5] Taub Institute for Research on Alzheimer's Disease and the Aging Brain, Columbia University Irving Medical Center, New York, NY, USA
[6] Department of Neuroscience, The Ohio State University Wexner Medical Center, Columbus, OH, USA
[7] Department of Biomedical Informatics, Ohio State Comprehensive Cancer Center, Columbus, OH, USA
[8] Department of Radiology, Division of Radiological Sciences, Washington University School of Medicine, St. Louis, MO, USA
[9] Knight Alzheimer Disease Research Center, Washington University School of Medicine, St. Louis, MO, USA
[10] Department of Neurology, Washington University School of Medicine, St. Louis, MO, USA
[11] Dominantly Inherited Alzheimer Network (DIAN)
[12] Department of Neurology, Indiana University School of Medicine, Indianapolis, IN, USA
[13] Department of Neurology, Massachusetts General Hospital, Harvard Medical School, Boston, MA, USA
[14] Department of Pediatrics, Columbia University, New York, NY, USA
[15] Department of Neurology, Beth Israel Deaconess, Harvard Medical School, Boston, MA, USA
[16] Department of Pathology and Immunology, Washington University School of Medicine, St. Louis, MO, USA
[17] Brain and Mind Centre, School of Medical Sciences, University of Sydney, Camperdown, NSW, Australia
[18] School of Medical Sciences and Charles Perkins Centre, Faculty of Medicine and Health, The University of Sydney, Sydney, NSW, Australia

*** Contributed equally**

[†] **Corresponding authors**

Abstract

Disrupted cross-cellular signaling (cellular crosstalk) is implicated in Alzheimer's disease (AD) and neurodegeneration. Previous studies were restricted to specific cell types and pathways, precluding a comprehensive understanding of cellular crosstalk in AD. Here, we systematically characterized crosstalk interactions using single-nucleus transcriptional profiles from 67 clinically and neuropathologically well-characterized controls and AD brain donors. Crosstalk between microglia and neurons involved known AD risk genes as ligands or receptors. Reconstruction of the gene networks mediating this crosstalk revealed additional known AD risk genes perturbed in microglia. We identified a novel interaction between neuronal SEMA6D and a microglial regulatory sub-network involving *TREM2* that is disrupted in AD and activated in the vicinity of Aβ plaques and *SEMA6D*-expressing cells. Using CRISPR-modified human induced pluripotent stem cell-derived microglia, we demonstrated that SEMA6D activates microglia in a TREM2-dependent manner. Together, we show that characterizing cellular crosstalk networks yields new insights into AD biology.

Introduction

Cross-cellular signaling (cellular crosstalk) is integral to normal brain physiology. By establishing cellular networks mediated by membrane receptors and their corresponding ligands, cells can gather information from their immediate environment and respond accordingly. Indeed, cellular crosstalk is crucial to brain homeostasis and processes of neurodevelopment, such as synaptic pruning and axon guidance[1,2]. However, increasing experimental and genetic evidence implicates aberrant cellular crosstalk as a contributing factor to neurodegenerative diseases[3–5]. A recent study characterized crosstalk interactions involving astrocytes and microglia in a mouse model of multiple sclerosis and identified a role for the plexin, semaphorin, and ephrin protein families in mediating neuroinflammation[5]. Another study identified a role for astrocyte-microglia crosstalk in modulating amyloid pathology[6]. Collectively, these studies indicate that maladaptive cellular crosstalk interactions contribute to neurodegeneration. Furthermore, from a translational perspective, cellular crosstalk is an attractive molecular target for drug development, as membrane receptors are relatively amenable to therapeutic targeting[7–9]. Therefore, systematic characterization of brain cellular crosstalk interactions can help identify molecular mechanisms involved in neurodegeneration and nominate novel treatments.

Genome-wide association studies (GWAS) have successfully identified genetic risk loci for Alzheimer's disease (AD) and the genes likely mediating these genetic signals[10–13]. Further, by leveraging human tissue[14–17] and experimental data from human induced pluripotent stem cell (iPSC)-derived cells[18], functional genomics studies have revealed that many AD risk genes are expressed by microglial cells. However, how most of these microglial AD risk genes are regulated in the contexts of normal physiology and AD pathophysiology is still unknown. As the resident immune cells of the brain, microglia are highly attuned to their surrounding environment, including signals from neighboring cells[19]. While previous studies have shown causal effects of disrupted crosstalk in neurodegeneration, it remains unclear how cellular crosstalk between microglia and other cell types is involved in mediating AD genetic risk. Understanding these processes requires techniques that can systematically characterize the

crosstalk networks in the brain, reconstruct the likely signaling pathways downstream of these interactions, and integrate these data with genetic findings.

In this study, we used single-nucleus transcriptomic profiles (snRNA-seq) from clinically, neuropathologically, and genetically well-characterized human brains to systematically reconstruct the cellular crosstalk networks across seven major brain cell types: microglia, astrocytes, oligodendrocytes, oligodendrocyte precursors (OPCs), excitatory and inhibitory neurons, and endothelial cells. We found that direct involvement of known AD risk genes was more frequent in neuron-microglia crosstalk interactions than in those between other cell types. In addition, we identified a sub-network of microglial genes centered around *TREM2* that we predicted mediates neuron-microglia crosstalk. We predicted that this sub-network is modulated by the crosstalk interaction between neuronal semaphorin 6D (SEMA6D) and microglial TREM2. We found evidence that this sub-network is disrupted in late-stage AD. Using spatial transcriptomics, we observed that the *TREM2* sub-network is activated in proximity to Aβ plaques and *SEMA6D*-expressing cells. Finally, we validated our predictions *in vitro* using wild-type (WT) and *TREM2* knockout (KO) human iPSC-derived microglia (iMGL). We showed that SEMA6D promotes microglia functions, including phagocytosis and cytokine release, in a TREM2-dependent manner. Our findings demonstrate that systematic characterization of cellular crosstalk networks in human brains is a viable strategy to elucidate aberrant regulatory biology in AD and other neurodegenerative diseases, which could ultimately lead to the development of effective AD therapies.

Results

A complex landscape of crosstalk dysregulation in AD

To systematically characterize cellular crosstalk interactions in controls and AD, we analyzed snRNA-seq profiles of superior parietal cortex tissue samples from brain donors of the Knight Alzheimer Disease Research Center (Knight ADRC) and the Dominantly Inherited Alzheimer Network (DIAN)[14]. This dataset encompasses different AD subtypes, including sporadic AD and autosomal dominant AD, with donors distributed in a broad spectrum of neuropathological states and genetic backgrounds, including carriers of *TREM2* risk variants **(Supp. Table 1)**. In total, we analyzed ~300K nuclei representing seven major brain cell types (microglia, astrocytes, oligodendrocytes, OPCs, excitatory and inhibitory neurons, and endothelial cells) from 67 donors (**Figure 1a**). We identified patterns of ligand-receptor gene expression across cell type pairs and their corresponding transcriptional states using CellPhoneDB[20], which has been successfully used to predict patterns of brain cellular crosstalk[5].

We detected condition-specific crosstalk interactions by stratifying brains by disease status and genetic group in our CellPhoneDB analyses. In total, we identified between 961 and 1,600 (median = 1,521) significant (Bonferroni-corrected $p < 0.05$) crosstalk interactions between cellular state pairs across all donor categories **(Figure 1b; Supp. Figure 1a; Supp. Table 2**). Furthermore, the observed crosstalk patterns remained similar with dataset downsampling, including removing a subset of donors, using a single donor, and using at most 100 barcodes per transcriptional state (fraction of replication 0.81 to 0.86, median = 0.84; **Supp. Figure 1a-d**). These results indicate that the crosstalk interaction patterns identified using CellPhoneDB are

highly robust to the number of donors, skews in donor representation, number of nuclei, and sequencing depth.

We compared the crosstalk patterns across donor categories to identify global changes associated with disease status. Overall, crosstalk interactions involving microglia with other cell types were significantly increased in all AD donors compared to controls (OR = 1.21, adj. *p* = 5.22e-4). In addition, we detected a significant decrease in crosstalk involving excitatory neurons with other cell types in sporadic AD donors (OR = 0.82, adj. *p* = 0.03; **Supp. Figure 2**). These results are consistent with neuronal loss and the critical role of microglia in AD.

We next performed a functional enrichment of the genes associated with the up- and down-regulated crosstalk interactions in each cell type to determine which crosstalk biological pathways are perturbed in AD. Consistent with widespread perturbations of normal brain physiology in AD, we observed changes in the cellular crosstalk patterns when comparing AD donors to controls. The crosstalk interactions up-regulated in AD were significantly enriched for pathways associated with immune activation and neuronal biology, including neuronal death (**Figure 1c**). Interestingly, we observed a significant increase in ephrin signaling in a subset of AD donors (*p* = 1.48e-12). These findings agree with the previously described role of the ephrin signaling pathway in neuroinflammation and neurodegeneration[5].

Aiming to understand how each cell type likely contributes to the dysregulated pathways in AD, we performed a similar functional enrichment analysis separately for the crosstalk interactions detected in each cell type. Interestingly, we observed that crosstalk interactions involving multiple cell types were enriched in immune activation and neuronal stress pathways, further supporting that cellular crosstalk contributes to these core features of neurodegeneration (**Supp. Figure 3**). Together, these results indicate that AD leads to widespread dysregulation of homeostatic cross-cellular signaling pathways between microglia and other cells.

Neuron-microglia crosstalk interactions are enriched to involve known AD risk genes as ligands or receptors

Our initial analysis identified thousands of significant crosstalk interactions across all cell types and donor categories. To identify interactions more likely to be directly involved in AD onset and progression, we next focused on interactions involving genes linked to AD by genetic and functional studies. We identified 90 possible crosstalk interactions directly involving an AD gene as the ligand or receptor (**Supp. Table 3**). Of these, 34 were significant by CellPhoneDB analyses in at least one cell type pair (**Figure 1d**). Microglia had the highest enrichment for crosstalk interactions involving AD genes when controlling for the total number of interactions ($\log_2$ OR range: 0.85 to 1.76, median = 1.23, *p* range: 4.69e-3 to 3.08e-8, median = 2.68e-4; **Figure 1e**). In addition, most AD gene interactions (64.9%) involved microglia as the likely receptor cell type (**Supp. Table 2**). To confirm that these results were not driven by the observed increase in crosstalk interactions involving microglia in AD vs. controls or the higher representation of AD genes in microglia compared to other cell types, we statistically controlled for these potential sources of bias and observed similar enrichment patterns (**Supp. Figure 4**, Methods). These results highlight that a subset of known AD genes is involved in crosstalk signaling between microglia and other cell types.

We next analyzed which cell types were most likely to interact with microglia via these crosstalk interactions involving AD genes. To do so, we performed conditional analyses by statistically conditioning the previous enrichments with microglia as one of the cell types. We observed that excitatory neurons had the highest enrichment point estimates to partner with microglia for crosstalk interactions involving AD genes but were only nominally significant in neuropathologically AD donors with no or minimal cognitive decline ($\log_2$ OR = 1.98, p = 0.035; **Figure 1f**). We replicated these analyses in three case-control snRNA-seq datasets of the prefrontal cortex region from the South West Dementia Brain Bank (SWDBB), the Rush ADRC, and the University of California Irvine Institute for Memory Impairments and Neurological Disorders (UCI MIND) ADRC (**Supp. Table 4**)[16,21,17]. We observed similarly strong enrichment of microglia for crosstalk interactions involving AD genes in all three studies ($\log_2$ OR range: 0.35 to 0.78, median = 0.71, p range: 0.025 to 7.53e-11, median = 1.63e-4; **Supp. Figure 5**). We observed differences across studies regarding the neuronal cell type (excitatory or inhibitory) most enriched for crosstalk interactions involving AD genes with microglia. Nonetheless, the enrichment direction of effect for excitatory neurons agreed with our findings in all studies. These results suggest that a subset of genes previously implicated in AD mediate cell signaling pathways between neurons and microglia.

To further validate that our previous results for AD were not driven by an overrepresentation bias of microglia interactions in the CellPhoneDB database, we calculated the enrichment of crosstalk interactions in genes nominated by GWAS for other neurological or neuropsychiatric traits (**Supp. Table 5**). In order for the results to be comparable between traits, we only used crosstalk interactions from the control donors from this study. If the crosstalk interactions observed in this study were biased towards one or a subset of cell types due to database overrepresentation, we would expect to observe similar enrichment patterns across traits. On the contrary, we observed distinct crosstalk enrichment patterns across neuropsychiatric traits (**Figure 1g**). For example, crosstalk interactions involving OPCs were significantly enriched for genes from one schizophrenia GWAS (OR = 2.64, adj. p = 3.12e-5). We also observed nominally significant enrichment for astrocyte crosstalk interactions for genes identified in Parkinson's disease GWAS (OR = 2.45, p = 0.029). Importantly, we replicated the enrichment for microglia crosstalk interactions in genes from two AD GWAS (Jansen *et al.* and Marioni *et al.* ORs = 3.39 and 3.07, adj. p = 3.16e-4 and 0.0023)[22,23]. We next used a strategy to nominate AD genes based on snATAC-seq co-accessibility between the gene promoter regions with a fine-mapped[12] AD GWAS variant (see Methods). This stringent approach nominates candidate AD genes and their corresponding cell types based solely on direct evidence from functional genomics. Despite microglia being among the least abundant cell types in the snATAC-seq dataset, we observed an approximately three-fold higher enrichment for microglia crosstalk interactions in AD (OR = 9.07, p = 1.24e-15; **Figure 1h**). These results indicate that the observed crosstalk enrichment patterns were not artificially biased toward any cell type. Furthermore, these analyses highlight that our crosstalk framework can be used to understand biological processes associated with GWAS variants for other neurological and neuropsychiatric diseases.

Microglia and excitatory neurons crosstalk interactions regulate additional known AD genes in microglia

We next sought to investigate how the crosstalk signals between neurons and microglia regulate gene regulatory networks downstream in microglia. Using a systems biology approach based on extending the functionality of the CytoTalk software[24] (see Methods), we reconstructed the gene co-expression networks upstream of the ligands and downstream of the receptors. CytoTalk is complementary to CellPhoneDB, as the latter does not inform the biological processes likely downstream of crosstalk interactions. Using CytoTalk, we reconstructed the gene regulatory network associated with crosstalk interactions between excitatory neurons and microglia (**Figure 2a-b**). Strikingly, the microglia co-expression network downstream of the neuron-microglia crosstalk interactions was enriched for genes previously associated with AD (cases OR range = 1.99 to 3.52, median = 3.06, adj. *p* range = 0.017 to 2.86e-8, median = 1.06e-4; **Figure 2c**). In addition, the microglia crosstalk network identified by CytoTalk was enriched for immune processes, including phagocytosis and cytokine production (**Figure 2d**), consistent with neuron-microglia crosstalk interactions modulating microglia activation states[25]. These results suggest that neuron-microglia crosstalk interactions propagate signals that modulate genes previously implicated in AD and involved in regulating microglial activation.

The SEMA6D-TREM2 crosstalk axis is predicted to modulate microglia activation

Among the seven crosstalk interactions prioritized by CytoTalk based on the co-expression network topology, we identified the crosstalk interaction between neuronal ligand semaphorin 6D (SEMA6D) and TREM2/TYROBP (DAP12) (**Figure 2b**). This crosstalk is mediated via PLXNA1[26]. However, *PLXNA1* was not included in the CytoTalk reconstructed network, possibly because of its low detection rate and limited dynamic range in our snRNA-seq data (only ~10% of microglia had detectable *PLXNA1* levels; max. *PLXNA1* expression = 3 reads). This is a reported limitation of snRNA-seq for lowly expressed genes[27,28] and precluded the reconstruction of its co-expression network by CytoTalk, resulting in a direct edge between *SEMA6D* and *TREM2/TYROBP* in the excitatory neuron-microglia network. Nonetheless, *PLXNA1* expression was sufficiently specific to microglia for CellPhoneDB and CytoTalk independently detect and prioritize the SEMA6D/PLXNA1/TREM2/TYROBP crosstalk interaction in our analyses.

Semaphorins and their receptors regulate immune cell function and are genetically and functionally implicated in AD[6,29–31]. In the brain, semaphorin signaling was initially described as a mediator of axon guidance via the plexin family of receptors[32]. However, a growing body of evidence indicates that these molecules are involved in immune responses[5,26,29,33–35]. Notably, a study in bone marrow-derived macrophages discovered that the SEMA6D-PLXNA1 interaction induces macrophage activation in a TREM2-dependent manner via the activation of DAP12[26]. Importantly, this study found that TREM2, PLXNA1, and TYROBP (DAP12) co-immunoprecipitate in a TREM2-dependent manner, consistent with the formation of a complex[36,37]. Furthermore, additional studies also linked plexin-semaphorin signaling to immune activation and neurodegeneration[5,35,38–40]. Given the role of SEMA6D in the immune activation of myeloid cells[26,40], we aimed to test the potential role of the SEMA6D-TREM2/PLXNA1 signaling axis in AD.

We identified a sub-network comprised of a clique of genes highly connected to *TREM2* and *TYROBP (DAP12)* by partitioning the microglia crosstalk network into sub-networks (Methods). Our crosstalk network reconstruction analysis predicted that this *TREM2* sub-network is the target of neuronal SEMA6D (**Figure 2e**). Furthermore, the *TREM2* sub-network was enriched for microglia activation pathways, indicating that we recapitulated the well-established link between TREM2 and microglia activation [41] through this unsupervised approach (**Figure 2d**). Interestingly, in addition to genes linked to microglia activation, the TREM2 crosstalk sub-network included *APOE* and *HLA* genes, previously reported as AD risk genes. The connection between *TREM2* and *APOE* is consistent with studies showing that APOE is a TREM2 ligand[42,43] and suggests that the TREM2-SEMA6D crosstalk interaction modulates AD risk genes.

To validate these results, we repeated the CytoTalk analyses in the snRNA-seq studies from the SWDBB, Rush ADRC, and UCI MIND ADRC cohorts[16,17,21]. Consistent with our results, CytoTalk prioritized the SEMA6D-TREM2 signaling axis mediating the crosstalk interactions between excitatory neurons and microglia in all three cohorts (**Supp. Figure 6a**). Finally, we determined that the *TREM2* sub-network and its predicted modulation by SEMA6D were robust to the choice of donors and the number of nuclei (**Supp. Figure 6b**). Together, these results reinforce that the unsupervised methodological approach in this study identified core elements of microglia gene regulation, which are predicted to be modulated by neuron-microglia cellular crosstalk interactions.

The microglia *TREM2* sub-network expression is negatively associated with advanced AD stages

We next sought to understand how the *TREM2* sub-network related to AD progression. We leveraged the wide range of neuropathological states in our dataset to develop a statistical framework to test the association of this sub-network gene expression level with disease severity while controlling for genetic and other confounding factors (Methods). We used high Braak stage (Braak ≥ IV) as a proxy of AD severity. Using this approach, we determined that the expression of the *TREM2* sub-network was negatively associated with high Braak stage (beta = -0.31, adj. p = 4.32e-57), indicating that this sub-network is disrupted in later AD stages. To understand this result within the broader context of all neuron-microglia crosstalk interactions, we calculated the association of all neuron-microglia crosstalk sub-networks with high Braak stage. Strikingly, the majority (11 of 14) of the microglia crosstalk sub-networks were negatively associated with high Braak stage, and the *TREM2* sub-network was among the most negatively associated with high Braak stage (**Figure 2f**). These results suggest that neuron-microglia crosstalk interactions and their downstream targets in microglia are impaired in the later stages of AD.

Next, we sought to determine if SEMA6D is a potential modulator of the *TREM2* microglia crosstalk sub-network. We reasoned that if this were the case, the neuronal *SEMA6D* crosstalk sub-network association with Braak stage would coincide with the *TREM2* sub-network. Indeed, the neuronal *SEMA6D* sub-network was negatively associated with high Braak stage (beta = -0.09, adj. p = 1.63e-04; **Figure 2g**). Therefore, our findings indicate that the biological processes associated with the SEMA6D-TREM2 neuron-microglia crosstalk interactions are

disrupted in AD and likely play a protective role by regulating TREM2-dependent microglia activation.

Multiple microglia co-expression sub-networks are disrupted during AD progression

To gain further insights into the role of microglia in AD, we next adapted the network analysis framework of CytoTalk to analyze the transcriptome-wide microglia co-expression network (*i.e.*, using all expressed genes in microglia; Methods). This approach allowed us to test the association of all microglia sub-networks with high Braak stage, regardless of the presence of reported ligands/receptors in the sub-networks. This broader reconstructed microglia co-expression network identified 360 sub-networks and independently recapitulated several crosstalk sub-networks in the previously described ligand-receptor prioritized analyses, including the *TREM2* sub-network (**Supp. Figure 7**). These microglia sub-networks were divided between positive and negative associations with high Braak stage (**Figure 2h; Supp. Table 6**). Consistent with the well-established roles of PSEN1 and APP in AD onset[44], the *PSEN1* and *APP* co-expression sub-networks were among the most positively correlated with high Braak stage (betas = 0.32 and 0.16, adj. p = 8.25e-57 and 2.17e-13, respectively). In contrast, the sub-network of *SORL1*, a gene associated with protective roles in AD[45,46], was negatively associated with Braak stage (beta = -0.15, adj. p = 3.52e-11). Interestingly, our unsupervised approach identified two separate sub-networks with opposing directions of effect for the genes in the MS4A locus, which genetically controls soluble TREM2 levels[47] (*MS4A4A* and *MS4A6A* betas = -0.11 and 0.19, adj. p = 2.87e-06 and 2.93e-20, respectively). This result suggests that the MS4A genetic signal regulates at least two independent biological processes, as we reported previously[47]. Notably, within the context of all microglia genes, the *TREM2* sub-network was among the most negatively associated with Braak stage (**Figure 2h**), consistent with our previous analysis. These results indicate that multiple biological pathways downstream of microglia-neuronal crosstalk are disrupted in AD. Furthermore, our unsupervised computational framework identified impaired TREM2-dependent microglia activation associated with AD progression.

The TREM2 sub-network expression correlates with proximity to Aβ plaques and is up-regulated in the presence of SEMA6D

Our previous findings that the *TREM2* sub-network was among the most negatively associated with advanced AD stages motivated us to better understand how its expression changed as a function of neuropathological burden. To do so, we reanalyzed spatial transcriptomics profiles (10X Genomics Visium) from three control and three AD (Braak III and IV) human brains[48] and quantified the effects of local neuropathology, in particular proximity to Aβ plaques, in relation to gene expression patterns (**Figure 2i**).

We first analyzed the global changes in gene expression between AD cases and controls and identified only 7 of 31 genes in the *TREM2* sub-network with nominal significant association (median $\log_2$ fold-change = 0.67; **Figure 2j-k)**. However, when we compared Aβ plaque-proximal to Aβ plaque-distal regions, we observed significant up-regulation of most genes in the *TREM2* sub-network (17 of 31 genes at least nominally significant, median $\log_2$ fold-change = 0.18). The spatially resolved data also showed a progressive overregulation of the *TREM2* sub-

network expression as a function of Aβ plaque proximity (**Supp. Figure 8a-b**), indicating that this pathway is likely involved in the immune response to amyloid pathology. Supporting this hypothesis, we observed that other gene signatures linked to plaque-associated microglia in single-cell transcriptomics studies of AD mouse models[15,49] were also overexpressed with Aβ proximity (**Supp. Figure 8c**).

Lastly, we leveraged the resolved spatial relationship of this dataset to test whether the *TREM2* sub-network expression levels changed in proximity to *SEMA6D*-expressing cells. In line with our single-cell analyses, we observed a significant up-regulation of the *TREM2* sub-network when comparing *SEMA6D*-positive versus *SEMA6D*-negative Visium spots (19 of 31 genes at least nominally significant; median $\log_2$ fold-change = 0.081; **Figure 2j-k**). The level of *TREM2* sub-network activation in proximity to *SEMA6D* was comparable between cases and controls (**Supp. Figure 8d**), suggesting that this crosstalk is overall active in earlier Braak stages. Together, these results suggest that the *TREM2* sub-network is involved in the response to Aβ plaques and is activated by SEMA6D.

SEMA6D induces immune activation in iPSC-derived microglia in a TREM2-dependent manner

To elucidate the role of SEMA6D-TREM2 crosstalk in microglia function, we used a human iPSC-derived microglia model[50] (iMGL; **Supp. Figure 9a**; Methods) that expresses established microglia markers, including TREM2, IBA1, and TMEM119 (**Supp. Figure 9b**). In addition, we generated *TREM2* KO human iPSCs using CRISPR/Cas9 to examine the role of the SEMA6D-TREM2 signaling axis on microglia function (**Supp. Figure 9c**). We verified the loss of TREM2 expression at the protein level in the KO cell line by western blot analysis (**Supp. Figure 9d**).

Because microglia regulate brain homeostasis through phagocytic activity and modulate neuroinflammation by releasing immune cytokines[51–53], we performed phagocytosis and cytokine assays (**Supp. Figure 10**). To determine if SEMA6D can regulate iMGL phagocytic activity and whether this process is TREM2 dependent, we treated WT and *TREM2* KO iMGL with recombinant SEMA6D protein. We measured the degree of phagocytic activity using pHrodo-labeled human synaptosomes as the phagocytic cargo. We observed increased phagocytosis in WT iMGL treated with SEMA6D starting at 6 hours of treatment with SEMA6D (1.3-fold change increase at 24 hours, p = 1.50e-8). In contrast, *TREM2* KO iMGL treated with SEMA6D had a less pronounced increase in phagocytosis compared to untreated *TREM2* KO cells (1.1-fold change increase at 24 hours, p = 0.001; **Figure 3a-b**; **Supp. Figure 11**). In parallel, we analyzed conditioned media of WT and *TREM2* KO iMGL using a multiplex immunoassay to determine if SEMA6D can regulate iMGL cytokine release. We found that SEMA6D increased the secretion of TNF-α by and IL-6 in WT but not *TREM2* KO iMGL (WT TNF-α and IL-6 fold-changes = 1.37 and 3.59, p = 4.58e-5 and 3.11e-5, respectively; **Figure 3c**). Together, these results indicate that SEMA6D increases iMGL phagocytosis and secretion of TNF-α and IL-6 cytokines in a primarily TREM2-dependent manner.

TREM2 mediates signaling through the adaptor protein TYROBP (DAP12), and the activation of TREM2 results in tyrosine phosphorylation within the ITAM motif and subsequent SYK phosphorylation[54]. To determine if SEMA6D activates TREM2 downstream signaling, we analyzed WT and *TREM2* KO iMGL protein lysates for phosphorylated SYK expression (p-SYK)

normalized to total SYK expression (SYK). Treatment of WT iMGL with SEMA6D induced a 1.84-fold increase in SYK phosphorylation (p = 0.0023), but these effects were not significant in *TREM2* KO iMGL (1.43-fold increase, p = 0.13; **Figure 3d-e**; **Supp. Figure 12**). These results demonstrate that SEMA6D can directly activate TREM2 signaling and suggests that SEMA6D signals through the TREM2/TYROBP (DAP12) complex (**Figure 3f**), although we cannot exclude that SEMA6D simultaneously activates other signaling pathways.

To systematically characterize the regulatory changes induced by SEMA6D treatment in iMGL, we generated bulk RNA-seq data for the SEMA6D-treated WT and *TREM2* KO iMGL and the corresponding untreated controls (**Supp. Figure 13**). We observed significant transcriptional changes associated with *TREM2* KO (n = 1,408 differentially expressed genes at 5% FDR; **Supp. Figure 13a-b**). As expected, *TREM2* was among the most downregulated genes in the *TREM2* KO iMGL (adj. p = 4.30e-22, rank = 26; **Supp. Figure 13a**). Strikingly, we observed robust transcriptional changes in SEMA6D-treated WT iMGL but not in SEMA6D-treated *TREM2* KO iMGL (n = 2,960 and 153 differentially expressed genes at 5% FDR, respectively; **Figure 3g; Supp. Figure 13a-b**), consistent with a pivotal role for TREM2 in mediating SEMA6D signaling in microglia. To further understand how TREM2 mediates this signaling pathway, we focused on the *TREM2* co-expression crosstalk sub-network predicted from the snRNA-seq data (**Figure 2e**). The *TREM2* sub-network had significantly lower expression in the untreated *TREM2* KO iMGL than WT (median $\log_2$ fold-change = -0.22, adj. p = 4.76e-04), consistent with TREM2 being a key regulator of this sub-network. In line with this interpretation, the *TREM2* sub-network was activated by SEMA6D treatment in the WT iMGL (median $\log_2$ fold-change = 0.40, adj. p = 7.50e-3) but significantly less so in the *TREM2* KO iMGL (median $\log_2$ fold-change = 0.06, adj. p = 0.040; **Figure 3h-i**). These results are consistent with the TREM2 signaling pathway being the primary mediator of SEMA6D in microglia but also suggest that SEMA6D can activate other pathways in microglia to a lesser extent.

We next analyzed biologically relevant transcriptional signatures previously described in microglia to gain further insights into how SEMA6D treatment regulates microglial transcriptional programs. These included genes up-regulated in phagocytosing microglia[52] and those up-regulated in response to LPS treatment[18]. As control signatures, we included genes down-regulated in another *TREM2* KO iMGL dataset[55] and a set of randomly selected genes for which we would not expect concerted transcriptional changes. We observed the strongest effects of SEMA6D treatment in the phagocytosing microglia gene signature (median $\log_2$FC = 0.47; **Figure 3i**), indicating that SEMA6D activates genes involved in phagocytosis in the WT but not *TREM2* KO iMGL. Notably, *TREM2*, *APOE*, and *RPS19* are among the most up-regulated genes by SEMA6D treatment in WT iMGL. These genes are either present in the phagocytosing microglia gene signature or correspond to genes previously linked to microglia activation[49,15] (**Figure 3j**). Our results indicate that SEMA6D-TREM2 crosstalk signaling induces a TREM2-mediated cascade of transcriptional events resulting in microglia activation.

Discussion

In this study, we leveraged single-nucleus gene expression profiles from a diverse cohort of brain donors to systematically dissect the contribution of cross-cellular signaling (cellular crosstalk) networks to AD. Our data-driven approach to identifying active crosstalk interactions

and reconstructing their corresponding downstream pathways provides additional evidence that disrupted cellular crosstalk networks contribute to neurodegeneration. One remarkable finding from our study is that a significant portion of AD risk genes is either directly involved in crosstalk interactions or immediately downstream of crosstalk interactions involving microglia. These results highlight the difficulty of characterizing the prominent role of microglia in AD, as the integration of complex signals originating in other brain cell types is core to their function. Specifically, our results support that dysregulation of the intricate signaling between neurons and microglia is linked to AD progression. Therefore, focusing on cellular crosstalk networks can provide further functional context to understand the biology of genes associated with AD risk in a cell-autonomous and non-autonomous manner.

Among the interactions we detected between neurons and microglia, we identified a novel functional link between neuronal SEMA6D and microglial TREM2. Furthermore, by leveraging iMGL, we demonstrated that SEMA6D signaling induces a TREM2-dependent microglia activation phenotype transcriptionally similar to phagocytosing microglia[52]. These results, combined with our observation that the transcriptional networks upstream and downstream of the SEMA6D-TREM2 interaction are downregulated in AD, suggest that loss of this crosstalk interaction exacerbates the deleterious processes occurring in the later stages of this disease.

We used iMGL to demonstrate that SEMA6D promotes microglial phagocytosis and inflammatory cytokine release. SEMA6D-induced microglial and downstream SYK activation were not observed in the *TREM2* KO iMGL. A previous study showed that SEMA6D promotes peripheral dendritic cell activation and osteoclast differentiation via the receptor complex harboring PLXNA1 and TREM2[56]. Thus, it is conceivable that SEMA6D functions as a natural ligand for the PLXNA1/TREM2 co-receptor and enhances TREM2 signaling in human microglia. Therefore, neuronal SEMA6D could influence functional properties and fate via the stimulation of TREM2-dependent intracellular signaling and induction of the *TREM2* gene expression network. Nevertheless, it remains to be determined if SEMA6D induces an anti-inflammatory state of microglia that might be beneficial in clearing neuropathological changes associated with AD.

SEMA6D also regulates lipid metabolism and polarization of macrophages via the interaction with another class A plexin family member, Plexin A4[33,57]. Several coding variants in PlexinA4 are associated with AD risk[33,58] and modulate both amyloid and tau pathology[38]. Thus, semaphorin-plexin signaling may play a fundamental role in regulating the functional interactions between excitatory neurons and a subset of microglia and may be perturbed in AD. Given that we observed weak transcriptional effects in iMGL associated with SEMA6D treatment in the absence of *TREM2*, it is possible that other proteins, such as Plexin A4, act as SEMA6D receptors. Therefore, future studies are necessary to determine the complete network of proteins mediating SEMA6D crosstalk in microglia.

While this study focused on a restricted subset of crosstalk interactions involving microglia and neurons, our systematic characterization of cross-cellular signaling patterns identified thousands of candidate interactions involving all brain cell types represented in our snRNA-seq data. Several of these interactions warrant further investigation. For example, the interleukin receptor IL1RAP has been previously implicated in genetic studies of AD endophenotypes[3,59–61], and the contribution of IL-1 signaling to neurodegenerative diseases has been well-established[62–64]. In

line with these previous findings, we identified the *IL1RAP* sub-network in microglia as the most negatively associated with Braak stage. These results suggest that the IL-1 signaling pathway disruption is likely involved in AD progression. More broadly, the IL1RAP case highlights that the continued exploration of brain crosstalk networks identified in this study will yield valuable biological insights into AD biology.

Finally, we identified distinct crosstalk enrichment patterns for genes identified by genetic studies of other neurological or neuropsychiatric traits. These results emphasize that cellular crosstalk is integral to normal brain physiology, and accounting for this regulatory layer will help contextualize how candidate disease risk genes fit into biological pathways. Together, our findings strongly support that the systematic characterization of cellular crosstalk networks is a viable strategy for gaining insight into the biology of neurodegenerative diseases and nominating targets for novel therapies.

Acknowledgments

Data collection and sharing for this project was supported by The Dominantly Inherited Alzheimer Network (DIAN, U19AG032438), funded by the National Institute on Aging (NIA), the Alzheimer's Association (SG-20-690363-DIAN), the German Center for Neurodegenerative Diseases (DZNE), Raul Carrea Institute for Neurological Research (FLENI), Partial support by the Research and Development Grants for Dementia from Japan Agency for Medical Research and Development, AMED, and the Korea Health Technology R&D Project through the Korea Health Industry Development Institute (KHIDI), Spanish Institute of Health Carlos III (ISCIII), Canadian Institutes of Health Research (CIHR), Canadian Consortium of Neurodegeneration and Aging, Brain Canada Foundation, and Fonds de Recherche du Québec – Santé. This manuscript has been reviewed by DIAN Study investigators for scientific content and consistency of data interpretation with previous DIAN Study publications. We acknowledge the altruism of the participants and their families and the contributions of the DIAN research and support staff at each participating site for their contributions to this study. The data available in the AD Knowledge Portal would not be possible without the participation of research volunteers and the contribution of data by collaborating researchers. The results published here are in whole or in part based on data obtained from the AD Knowledge Portal (https://adknowledgeportal.org). This research was supported by NIH grants R01AG067606 (TWK), U01AG072464 (CMK, OH), NINDS R01NS118146 and R21NS127211 (to BAB), NIH R01AG062734 (CMK), R56AG067764 (GS), NIA R01AG075092 (HF), P30AG066444 (JCM), P01AGO26276 (JCM), and P01AG003991 (JCM). Additional funding from the Chan Zuckerberg Initiative (CMK, OH, CC) and the Department of Defense (W81XWH1910309 to HF). O.H. is an Archer Foundation Research Scientist. This work was supported by access to equipment made possible by the Hope Center for Neurological Disorders and the Departments of Neurology and Psychiatry at Washington University School of Medicine. We thank Barbara Corneo for advice on iPSC protocols and Wei Wang and Caisheng (Luke) Lu, MD, Ph.D., for assisting FACS sorting. iMGL cell sequencing and preliminary RNA-seq data processing were conducted by Novogene.

Author contributions

RDA analyzed data, designed and performed computational experiments, wrote the manuscript. GMF analyzed data, designed and performed iPSC experiments, wrote the manuscript. LB performed initial snRNA-seq quality control, cell clustering, and integration with public datasets. SC annotated spatial transcriptomics data. QG performed spatial transcriptomics deconvolution. AK designed and performed experiments, analyzed data, and revised the manuscript. MA performed experiments and revised the manuscript. SFY performed computational experiments. BCN performed initial snRNA-seq processing quality control. PMRP revised the manuscript. DMH revised the manuscript. JCM supervised sample acquisition and revised manuscript. EMD supervised sample acquisition, revised manuscript. MF supervised sample acquisition and revised the manuscript. JPC supervised sample acquisition, revised manuscript. RJP supervised and participated in sample acquisition, performed neuropathological assessments, and revised the manuscript. EEM contributed to experimental data acquisition. BAB analyzed data, supervised snRNA-seq data generation, and revised the manuscript. LP conceptualized results and revised the manuscript. GTS supervised sample and genetic data acquisition, revised manuscript. QM supervised spatial transcriptomics computational analyses. HF: Supervised sample acquisition and revised manuscript. CMK supervised experimental data acquisition and revised the manuscript. OH conceptualized and designed computational experiments, analyzed data, supervised and edited the manuscript, and supervised all aspects of the project. TWK conceptualized and designed iPSC experiments, analyzed data, supervised and edited the manuscript, and supervised all aspects of the project.

Competing interests

TWK is a cofounder of BL Melanis Co. Ltd. DMH co-founded and is on the scientific advisory board of C2N Diagnostics. DMH consults for Genentech, Denali, Cajal Neurosciences, and Alector. JCM. is a consultant for the Barcelona Brain Research Center (BBRC) and the TS Srinivasan Advisory Board. JCM. is a consultant for the Barcelona Brain Research Center (BBRC) and the TS Srinivasan Advisory Board. JCM. is an advisory board member for the Cure Alzheimer's Fund Research Strategy Council. JCM. receives research support from the NIH and the Alzheimer's Association (US) and is a member of the advisory board for Humana Healthcare. EMD. receives research support from the NIA, Hoffman-LaRoche, and Eli Lilly, is a member of advisory boards for Eli Lilly, Alector, and the NIA, and holds a leadership role in Fondation Alzheimer and Alzamend. The remaining authors have no competing interests related to this study.

Methods

snRNA-seq data processing

We reanalyzed single-nucleus transcriptomic profiles (snRNA-seq) of superior parietal cortex tissue samples from 67 donors of the Knight Alzheimer Disease Research Center (Knight ADRC) and the Dominantly Inherited Alzheimer Network (DIAN)[14]. Samples were previously obtained with informed consent for research use and were approved by the review board of Washington University in St. Louis. AD neuropathological changes were assessed according to the National Institute on Aging-Alzheimer's Association (NIA-AA) criteria. Demographic, clinical

severity and neuropathological information are available in our original study[14]. Briefly, we used the 10X Chromium single-cell Reagent Kit v3, aiming for 10,000 nuclei per individual and 50,000 reads per nucleus, as recommended by 10X Genomics. We mapped the sequenced reads to the GRCh38 human reference genome using CellRanger (v. 6.1.1) and filtered nuclei based on sequencing depth and percent mitochondrial reads. We obtained snRNA-seq data from 294,114 nuclei after stringent QC[14,65] (median nuclei per donor after QC = 3,637). We used Seurat[66] (v. 3.2.3) to identify cell types and transcriptional states using previously described cell type markers[67].

We obtained the count matrices and barcode metadata from three other public snRNA-seq datasets from human brains[16,17,21] as made available by the authors. We used the existing barcode metadata from these studies to annotate the nuclei into cell types and donor groups (*e.g.*, AD, controls). We considered any nuclei not in the final metadata table for the respective study as failing QC. These nuclei were discarded from downstream analyses. In order to run CellPhoneDB and CytoTalk in these datasets, we normalized each study separately using the SCT normalization[68] from Seurat.

Reanalysis of brain snATAC-seq data

We downloaded the raw snATAC-seq fastq files from the Morabito *et al.* study[17] and re-processed this dataset using CellRanger-ATAC (v. 2.0.0) count function. First, we filtered the resulting GRCh38 BAM files for each sample using flags *-f 3 -F 4 -F 8 -F 256 -F 1024 -F 2048 -q 30* to retain high-quality, properly mapped alignments. Second, we split each sample BAM file into separate files corresponding to each cell type using the barcode annotations reported by the authors. Then, for each cell type, we merged all BAM files across donors and called narrow peaks using MACS2 (v. 2.2.7.1)[69] using flags *--nomodel --shift -100 --extsize 200 --keep-dup all --call-summits -B*. Third, we filtered all peaks overlapping the GRCh38 ENCODE exclusion list regions (ENCODE accession ENCFF356LFX)[70]. Finally, we used CICERO[71], with default parameters, to calculate co-accessibility across ATAC-seq narrow peaks for each cell type separately.

Cell Culture

Human iPSCs were maintained feeder-free on matrigel-coated plates in StemFlex medium (Gibco) in a humidified incubator (5% CO_2, 37 °C). Cells were passaged as aggregates using ReLeSR (StemCell Technologies), and media was changed daily.

Differentiation of iPSC to iPSC-derived microglia (iMGL)

iPSC-microglia were generated as described in McQuade et al., 2018[50]. Briefly, iPSCs were directed down a hematopoietic lineage using the STEMdiff Hematopoietic kit (STEMCELL Technologies). After 12 days in culture, hematopoietic progenitor cells (HPCs) were transferred into a microglia differentiation medium containing DMEM/F12, 2× insulin-transferrin-selenite, 2× B27, 0.5× N2, 1× GlutaMAX, 1× nonessential amino acids, 400 μM monothioglycerol, and 5 μg/mL human insulin. Media was added to cultures every other day and supplemented with 100 ng/mL IL-34, 50 ng/mL TGF-β1, and 25 ng/mL M-CSF (PeproTech) for 28 days. In the final three days of differentiation, 100 ng/mL CD200 (Novoprotein) and 100 ng/mL CX3CL1 (PeproTech) were added to the culture.

Generation of TREM2 KO iPSCs

The WT iPSC line (APOE 3/3) was a generous gift from Dr. Barbara Corneo[72]. TREM2 KO iPSCs were generated using the Human Stem Cell Nucleofector™ Kit 2 (Lonza) according to the manufacturer's protocol. Briefly, iPSCs were resuspended in 100 µL nucleofection buffer and 5 µg of vector lentiCRISPRv2GFP expressing sgRNA against TREM2 (5'ATCACAGACGATACCCTGGG 3'). LentiCRISPRv2GFP was a generous gift from David Feldser (Addgene plasmid# 82416; http://n2t.net/addgene:82416; RRID:Addgene_82416). The suspension was transferred to the Amaxa Nucleofector cuvette and transfected using program CA-137. GFP-expressing cells were single-cell sorted into 96-well plates using the BD Influx cell sorter (Columbia University CCTI/HICCC Flow Core). Cell colonies were maintained and expanded. TREM2 KO cell lines were verified by Sequencing (Genewiz).

Flow Cytometry

iMGL cells were suspended in FACS buffer (DPBS, 2% BSA, 50 µM EGTA) and treated with FC block (1:50, BD Biosciences 564219) for 20 min at 4 °C. Cells were centrifuged and resuspended in FACS buffer before adding CD11b-PE/Cy5 (1:100, Biolegend 101209), CD45-BV650 (1:50, Biolegend 304043), or TREM2-APC (1:50, R&D Systems FAB17291A) and incubated 30 min at 4 °C in the dark. Samples were washed 3× in FACS buffer. Cells were resuspended in FACS buffer and stained with DAPI. Cells were analyzed with the BD Influx Cell Sorter.

Western Blotting Analysis and Antibodies

Proteins were resolved via SDS-PAGE using NuPAGE™ 4-12% Bis-Tris gels (Invitrogen) and probed for expression. Proteins were detected using the Odyssey XF Imager (LI-COR Biosciences). Antibodies used included: anti-Phospho-SYK (Cell Signaling), anti-SYK (Cell Signaling), anti-TREM2 (Cell Signaling), and anti-β-actin (Sigma).

Immunocytochemistry

iMGL were fixed in 4% paraformaldehyde, permeabilized, and blocked for 1 hr in 10% normal goat serum or 10% fetal bovine serum. Primary antibodies were diluted in 10% normal goat serum containing 0.1% Triton X-100 and incubated overnight at 4°C. Primary antibodies included anti-TREM2 (R&D Systems), anti-IBA1 (Fujifilm), and anti-TMEM119 (Novus)). Following incubation of the primary antibody, cells were washed and incubated for 1 hr at room temperature in Alexa Fluor 568- or 488-conjugated secondary antibody (Invitrogen). Immunostained cells were mounted using VECTASHIELD Mounting Medium (Vector Laboratories) and imaged using the Nikon C1 Digital Confocal System.

Synaptosome Preparation

The human temporal lobe was homogenized using a Dounce tissue grinder in homogenization buffer (0.032 M Sucrose, 0.5 mM $CaCl_2$, 1 mM $MgCl_2$, 1 mM $NaHCO_3$ supplemented with protease/phosphatase inhibitor) and centrifuged at 1400×g. The supernatant was saved (S1), and the resulting pellet was re-homogenized in homogenization buffer and centrifuged at 700×g, resulting in the supernatant, S1'. Supernatants S1 and S1' were mixed and centrifuged at 700×g resulting in the supernatant, S2. S2 was centrifuged at 14000×g. The resulting pellet containing synaptosomes was resuspended in buffer (0.32 M Sucrose, 1 mM $NaHCO_3$).

Oligomer and fibril formation

Aβ42 oligomers and fibrils were prepared according to the established protocol by Stine *et al*.[73]. Briefly, Aβ42 (Anaspec) was resuspended to 1 mM solution in HFIP. Aliquots were evaporated in a fume hood for 2 hrs, and the resulting peptide film was dried under vacuum in a SpeedVac and stored at -20°C. Immediately prior to use, the films were solubilized to 1 mM in anhydrous DMSO, sonicated in a bath sonicator for 10 min, and diluted to 100 µM in oligomer-forming conditions (cold PBS; incubation at 4°C for 24 h) or fibril-forming conditions (10mM HCl; incubation at 37°C for 24 h).

pHrodo Labeling

pHrodo Red (Invitrogen) labeling protocol was adapted from the manufacturer's instructions. Briefly, Aβ42 oligomer or fibril solutions (100 µM) were centrifuged at 16000×g for 2 min to collect the aggregates. Aggregates were washed in 1 mL HBSS and centrifuged for 2 min. The supernatants were aspirated, and 200 µl of pellet aggregates were resuspended by adding 200 µl 0.1M $NaHCO_3$ to the pellets. The pHrodo Red dye (10 mg/ml) was then added per the manufacturer's instructions. pHrodo labeling was performed and incubated for 1 hr in the dark, followed by centrifugation at 16000×g for 2 min. Aggregates were washed 3x with HBSS and resuspended to 100 µM in HBSS.

Phagocytosis assay

iMGL were plated at a density of $3x10^5$ cells per well in 96-well plates and incubated for 24 hrs. iMGL were treated with 10 µM SEMA6D in media supplemented with either 30 µg/ml pHrodo Red tagged synaptosomes, 1 mM pHrodo Red tagged Aβ fibril or 400 nM Aβ oligomer and incubated for 24 hrs. Cells were imaged using an IncuCyte live cell imaging system. Analysis was performed by Incucyte Zoom Software. The phagocytic activity of iMGL was quantified using the Incucyte® SX5 Live-Cell Analysis instrument**.** Total cell counts were performed using the CellQuanti-Blue™ Cell Viability Assay kit (BioAssay Systems). Three independent experiments were performed, where all four experimental conditions (WT, KO, WT+SEMA6D, and KO+SEMA6D) were assayed in triplicate (three wells) per experiment. To obtain significance values for Figure 3b, we used the sumz function from the R metap package (v. 1.8).

Cytokine assay

iMGL were plated at a density of $3x10^5$ cells per well in 96-well plates and incubated for 24 hrs. iMGL were treated with 10 µM SEMA6D or 1uM LPS for 24 hrs. Cell media was harvested, and cytokines were quantified using the V-PLEX Human Proinflammatory Panel II (4-Plex) (MSD) according to the manufacturer's instructions. Total cell counts were performed using the CellQuanti-Blue™ Cell Viability Assay kit. Because these experiments were performed in three batches, we analyzed the effects of SEMA6D treatment in cytokine secretion using a linear regression model, including a covariate for the experiment batch.

iMGL RNA-seq

WT or TREM2 KO iMGL were treated with 10 µM SEMA6D for 24 hrs. mRNA was extracted from iMGL using RNeasy Mini kit (Qiagen) following the manufacturer's instructions. Human mRNA sequencing and bioinformatics analysis were performed by Novogene. Raw fastq files were mapped to the GRCh38 reference genome using HISAT2 (v. 2.0.5)[74] and the

corresponding GRCh38 index files (http://daehwankimlab.github.io/hisat2/download). We used DESeq2[75] for differential analyses. Briefly, we retained genes with ≥ 10 counts in at least three samples and processed all samples together to increase the statistical power to calculate dispersion. We then retrieved the fold changes and significances for the comparisons of interest individually (*e.g.*, SEMA6D-treated WT vs. untreated WT). Finally, we adjusted for multiple testing per comparison using the Benjamini-Hochberg correction[76] and used a 10% false discovery rate (FDR) threshold to identify differentially expressed genes.

CellPhoneDB analyses

We used CellPhoneDB[20] (v. 2.1.7) to estimate crosstalk interactions based on the expression of known ligand-receptor pairs. We used the *cellphonedb method statistical_analysis* function with default parameters to calculate crosstalk interactions at the cluster level (transcriptional state) using the sctransform-normalized snRNA-seq count matrices as input. We performed CellPhoneDB analyses for each subset of donors separately (*e.g.*, controls, sporadic AD). We considered significant all those interactions that passed multiple testing correction (Bonferroni $p < 0.05$) for the entire set of analyses (all transcriptional states and donor categories).

To address potential bias from differences in cell type representation, we performed an additional CellPhoneDB analysis, downsampling each cluster in our snRNA-seq data to 100 nuclei barcodes. Similarly, we re-ran CellPhoneDB in multiple combinations of two to three cell types in our data (e.g., astrocytes and OPC only, astrocytes, microglia, and OPC only) to confirm that the resulting interactions were stable across subsets of cell types. Finally, we repeated the CellPhoneDB analyses individually for a subset of brains to confirm that the crosstalk patterns were identified at a single brain level. For other public snRNA-seq datasets analyzed in this study, we used the cluster and donor labels provided by the authors of each study.

To calculate the significance of CellPhoneDB interactions, we used Fisher exact tests (FETs) to compare the number of interactions at the cell type level. We used the union of all significant interactions across transcriptional states for each cell type. We generated one 2x2 contingency table per cell type and donor category combination to compare controls versus other donor categories. One dimension of the contingency table encoded the number of unique significant CellPhoneDB interactions involving the cell type of interest versus all other cell types combined. The other dimension encoded the number of interactions identified in the controls versus the donor category of interest. To calculate the enrichment of crosstalk interactions involving AD-related genes per cell type, we generated, for each donor category, 2x2 contingency tables encoding the number of interactions involving the cell type of interest (yes versus no) and involving AD genes (yes versus no). Finally, we calculated the enrichment of AD-related crosstalk interactions pairwise across all cell-type pairs by further subsetting the previous contingency tables to separate between AD-related interactions involving cell type of interest A and cell type of interest B versus cell type of interest A without cell type of interest B (*e.g.*, microglia and excitatory neurons versus to microglia and the remaining cell types). All FET p-values were corrected for multiple testing using the Bonferroni correction based on the total number of tests performed for each analysis.

Crosstalk enrichments for other neuropsychiatric traits

We downloaded the GWAS associations of neuropsychiatric traits from the European Bioinformatics Institute GWAS catalog (https://www.ebi.ac.uk/gwas) for the studies listed in **Supp. Table 5**. We used the mapped genes for each locus as the input gene list to calculate the crosstalk enrichments in each study. We used the same FET approach described above for the AD-related crosstalk interactions to calculate the enrichment of genes nominated by each GWAS study (**Figure 2d**). To calculate the enrichment of crosstalk interactions involving genes associated with AD GWAS based on co-accessibility (**Figure 2e**), we used as the input gene list all genes with a transcription start site (TSS) region either 1) overlapping an ATAC-seq peak co-accessible with another ATAC-seq peak harboring a fine-mapped AD GWAS variant (PPA > 0.01) from the Schwartzentruber *et al.* study[12] or 2) overlapping an ATAC-seq peak in any cell type harboring a fine-mapped variant.

Downstream crosstalk networks reconstruction using CytoTalk

We used CytoTalk (v. 4.0.3) with minor modifications to identify the signaling networks downstream of crosstalk interactions. CytoTalk first reconstructs the co-expression network of two cell types using information theory, then prioritizes biologically relevant crosstalk interactions based on their connection to central genes in each network using graph theory. This analysis results in a prioritized network of genes predicted to mediate the crosstalk signals between the two cell types. Briefly, CytoTalk reconstructs the co-expression network for each cell type pair and connects them based on a database of ligand-receptor interactions. It then uses a prize-collecting Steiner forest algorithm to identify the crosstalk signaling network between the two cell types[24]. We generated input csv files per cell type for each donor category containing the sctransform-normalized snRNA-seq log-transformed counts per barcode. Additionally, we increased the stringency of the CytoTalk networks by manually inputting only interactions that were also present in CellPhoneDB. This step was done because CytoTalk uses protein-protein interactions and text mining from STRING-DB[77] to build its crosstalk interactions database, which we consider overly permissive. For the network visualization in **Figure 2a**, we used the union of the crosstalk signaling network identified for each donor category in microglia versus excitatory neurons. We generated network visualizations using Cytoscape (v. 3.9.0)[78] and identified crosstalk sub-networks using the community cluster (GLay) function of clusterMaker (v. 2.2)[79]. The modified CytoTalk version used in this study (https://github.com/rdalbanus/CytoTalk) fixed minor bugs and enabled better parallelization control for a cluster environment. These issues have since been fixed in newer CytoTalk releases.

To calculate the enrichment of AD-related genes downstream of the crosstalk interactions (**Figure 2c**), we used FETs to compare the number of AD-related genes in each side of the excitatory neuron-microglia crosstalk network versus all AD-related genes expressed in the corresponding cell type. All FET p-values were corrected for multiple testing using the Bonferroni correction based on the total number of tests performed for each analysis.

Network analyses

We used the *compute_mutual_information_single* function from CytoTalk to reconstruct the excitatory neurons and microglia co-expression networks for each donor category. Briefly, this

function calculates the mutual information (MI)[80] across all pairs of genes per cell type and then applies the ARACNE algorithm[81] to eliminate most indirect interactions between genes. We then merged the ARACNE-filtered MI matrices for each cell type across donor categories by keeping the highest MI value for each interaction. In order to identify co-expression sub-networks, we applied the WGCNA pipeline[82] on the merged MI matrix. To test the association of each sub-network (n = 360) with the Braak stage, we first calculated its eigengene (the first principal component of gene expression) for each sub-network. We then tested the association of each eigengene with a high Braak stage using the binomial regression model:

$$Braak\ high_i \sim eigengene_{ij} + sex_i + APOE4_i + TREM2_i$$

In this model, i represents a barcode and j, a co-expression sub-network. $Braak\ high_i$, sex_i, $APOE4_i$, and $TREM2_i$ are binary variables encoding the donor Braak stage (Braak > III versus Braak ≤ III), sex, *APOE* genotype (one or two copies of *APOE4* versus zero), and *TREM2* genotype (common variant versus R47H, R136W, or R62H). We ran this model for each sub-network and obtained the corresponding coefficient and p-value of the eigengene term. Then, we adjusted the significance for multiple testing using the Bonferroni correction. Similarly, we performed this same analysis in the sub-networks obtained from the CytoTalk microglia-excitatory neurons crosstalk network.

Spatial transcriptomics

We processed the raw count matrices from the 10X Genomics Visium data as described in the original study[48]. Briefly, we used only spots that passed QC in the original study and applied the SCT integration pipeline from Seurat to integrate data across donors. All differential expression analyses were performed using NEBULA[83], using covariates for the donor of origin (random effects model) and the previously calculated proportion of neurons and microglia using Cell2location[84] for each Visium spot. All spots were previously manually annotated regarding the presence of Aβ plaques based on immunostaining from immediately adjacent tissue slices. For the comparisons between Aβ-proximal versus distal spots, we defined as Aβ-proximal spots any spot that directly overlapped Aβ plaques, and we defined as Aβ-distal spots any spot that was more than four spots away from the nearest Aβ-proximal spot. For the *SEMA6D*-positive versus -negative comparisons, we used a threshold of ≥1 SCT-normalized *SEMA6D* reads to separate between classes. For cases versus controls, we used all the spots for each donor.

Functional enrichments

All gene ontology (GO) functional enrichments in this study were calculated with the WebGestaltR R package (v. 0.4.4), using the *ORA* method, the *geneontology_Biological_Process_noRedundant* annotation, and the *genome_protein-coding* reference set. For all analyses, we used an FDR threshold of 1 to recover all enrichments and manually adjusted p-values for multiple testing using the Bonferroni correction (significance threshold used: $p < 0.05$). We used the R package rrvgo (v. 1.9.1) to collapse redundancy in GO terms further. For each WebGestaltR analysis, we generated a similarity matrix across all GO terms significant in at least one comparison using the *calculateSimMatrix* function. We then reduced the significant terms for each analysis using the *reduceSimMatrix* function. The *threshold* values for the *reduceSimMatrix* function were selected based on visual inspection of

the resulting terms (0.8 for the analyses in Figures 1F and 3C and 0.9 for Figure 3F). Finally, we reported the most significant p-value among the grouped terms under each parent term.

Data availability

Human iMGL bulk RNA-seq data is currently awaiting GEO approval for submission. Reviewer tokens will be made available once the data is deposited. The snRNA-seq data from the Knight ADRC is publicly available by request from the National Institute on Aging Genetics of Alzheimer's Disease Data Storage Site (NIAGADS) under accession number NG00108 (https://www.niagads.org/datasets/ng00108). DIAN brain bank snRNA-seq data access requires a request through https://dian.wustl.edu/our-research/for-investigators.

Code availability

All scripts necessary to reproduce the figures from this manuscript will be available at https://github.com/albanus-research/2021_trem2_adad_snRNAseq. The modified CytoTalk version used for this manuscript is available at https://github.com/rdalbanus/CytoTalk.

References

1. Schafer, D. P. *et al.* Microglia sculpt postnatal neural circuits in an activity and complement-dependent manner. *Neuron* **74**, 691–705 (2012).
2. Fard, D. & Tamagnone, L. Semaphorins in health and disease. *Cytokine Growth Factor Rev* **57**, 55–63 (2021).
3. Ramanan, V. K. *et al.* GWAS of longitudinal amyloid accumulation on 18F-florbetapir PET in Alzheimer's disease implicates microglial activation gene IL1RAP. *Brain* **138**, 3076–3088 (2015).
4. McAlpine, C. S. *et al.* Astrocytic interleukin-3 programs microglia and limits Alzheimer's disease. *Nature* (2021) doi:10.1038/s41586-021-03734-6.
5. Clark, I. C. *et al.* Barcoded viral tracing of single-cell interactions in central nervous system inflammation. *Science* **372**, eabf1230 (2021).
6. Lian, H. *et al.* Astrocyte-Microglia Cross Talk through Complement Activation Modulates Amyloid Pathology in Mouse Models of Alzheimer's Disease. *J Neurosci* **36**, 577–589 (2016).
7. Yin, H. & Flynn, A. D. Drugging Membrane Protein Interactions. *Annu Rev Biomed Eng* **18**, 51–76 (2016).
8. Overington, J. P., Al-Lazikani, B. & Hopkins, A. L. How many drug targets are there? *Nat Rev Drug Discov* **5**, 993–996 (2006).
9. Worzfeld, T. & Offermanns, S. Semaphorins and plexins as therapeutic targets. *Nat Rev Drug Discov* **13**, 603–621 (2014).
10. Lambert, J. C. *et al.* Meta-analysis of 74,046 individuals identifies 11 new susceptibility loci for Alzheimer's disease. *Nat Genet* **45**, 1452–1458 (2013).
11. Kunkle, B. W. *et al.* Genetic meta-analysis of diagnosed Alzheimer's disease identifies new risk loci and implicates Aβ, tau, immunity and lipid processing. *Nat Genet* **51**, 414–430 (2019).
12. Schwartzentruber, J. *et al.* Genome-wide meta-analysis, fine-mapping and integrative prioritization implicate new Alzheimer's disease risk genes. *Nat Genet* **53**, 392–402 (2021).
13. Bellenguez, C. *et al.* New insights into the genetic etiology of Alzheimer's disease and related dementias. *Nat Genet* (2022) doi:10.1038/s41588-022-01024-z.

14. Brase, L. *et al. A landscape of the genetic and cellular heterogeneity in Alzheimer disease*. http://medrxiv.org/lookup/doi/10.1101/2021.11.30.21267072 (2021) doi:10.1101/2021.11.30.21267072.
15. Olah, M. *et al.* Single cell RNA sequencing of human microglia uncovers a subset associated with Alzheimer's disease. *Nat Commun* **11**, 6129 (2020).
16. Lau, S.-F., Cao, H., Fu, A. K. Y. & Ip, N. Y. Single-nucleus transcriptome analysis reveals dysregulation of angiogenic endothelial cells and neuroprotective glia in Alzheimer's disease. *Proc Natl Acad Sci U S A* **117**, 25800–25809 (2020).
17. Morabito, S. *et al.* Single-nucleus chromatin accessibility and transcriptomic characterization of Alzheimer's disease. *Nat Genet* (2021) doi:10.1038/s41588-021-00894-z.
18. Dräger, N. M. *et al. A CRISPRi/a platform in iPSC-derived microglia uncovers regulators of disease states*. http://biorxiv.org/lookup/doi/10.1101/2021.06.16.448639 (2021) doi:10.1101/2021.06.16.448639.
19. Li, Q. & Barres, B. A. Microglia and macrophages in brain homeostasis and disease. *Nat Rev Immunol* **18**, 225–242 (2018).
20. Efremova, M., Vento-Tormo, M., Teichmann, S. A. & Vento-Tormo, R. CellPhoneDB: inferring cell–cell communication from combined expression of multi-subunit ligand–receptor complexes. *Nat Protoc* **15**, 1484–1506 (2020).
21. Zhou, Y. *et al.* Human and mouse single-nucleus transcriptomics reveal TREM2-dependent and TREM2-independent cellular responses in Alzheimer's disease. *Nat Med* **26**, 131–142 (2020).
22. Jansen, I. E. *et al.* Genome-wide meta-analysis identifies new loci and functional pathways influencing Alzheimer's disease risk. *Nat Genet* **51**, 404–413 (2019).
23. Marioni, R. E. *et al.* GWAS on family history of Alzheimer's disease. *Transl Psychiatry* **8**, 99 (2018).
24. Hu, Y., Peng, T., Gao, L. & Tan, K. CytoTalk: De novo construction of signal transduction networks using single-cell transcriptomic data. *Sci. Adv.* **7**, eabf1356 (2021).
25. Szepesi, Z., Manouchehrian, O., Bachiller, S. & Deierborg, T. Bidirectional Microglia-Neuron Communication in Health and Disease. *Front Cell Neurosci* **12**, 323 (2018).
26. Takegahara, N. *et al.* Plexin-A1 and its interaction with DAP12 in immune responses and bone homeostasis. *Nat Cell Biol* **8**, 615–622 (2006).
27. Thrupp, N. *et al.* Single-Nucleus RNA-Seq Is Not Suitable for Detection of Microglial Activation Genes in Humans. *Cell Rep* **32**, 108189 (2020).
28. Wang, X., He, Y., Zhang, Q., Ren, X. & Zhang, Z. Direct Comparative Analyses of 10X Genomics Chromium and Smart-seq2. *Genomics Proteomics Bioinformatics* **19**, 253–266 (2021).
29. Kumanogoh, A. & Kikutani, H. Immunological functions of the neuropilins and plexins as receptors for semaphorins. *Nat Rev Immunol* **13**, 802–814 (2013).
30. Jun, G. *et al.* PLXNA4 is associated with Alzheimer disease and modulates tau phosphorylation. *Ann Neurol* **76**, 379–392 (2014).
31. Good, P. F. *et al.* A role for semaphorin 3A signaling in the degeneration of hippocampal neurons during Alzheimer's disease. *J Neurochem* **91**, 716–736 (2004).
32. Nakamura, F., Kalb, R. G. & Strittmatter, S. M. Molecular basis of semaphorin-mediated axon guidance. *J Neurobiol* **44**, 219–229 (2000).
33. Kang, S. S. *et al.* Identification of plexin A4 as a novel clusterin receptor links two Alzheimer's disease risk genes. *Hum Mol Genet* **25**, 3467–3475 (2016).
34. Evans, E. E. *et al.* Semaphorin 4D is upregulated in neurons of diseased brains and triggers astrocyte reactivity. *J Neuroinflammation* **19**, 200 (2022).
35. Ito, T. *et al.* Plexin-A1 is required for Toll-like receptor-mediated microglial activation in the development of lipopolysaccharide-induced encephalopathy. *Int J Mol Med* **33**, 1122–1130 (2014).

36. Klesney-Tait, J., Turnbull, I. R. & Colonna, M. The TREM receptor family and signal integration. *Nat Immunol* **7**, 1266–1273 (2006).
37. Kober, D. L. & Brett, T. J. TREM2-Ligand Interactions in Health and Disease. *J Mol Biol* **429**, 1607–1629 (2017).
38. Chung, S. *et al.* Plexin-A4 mediates amyloid-β-induced tau pathology in Alzheimer's disease animal model. *Prog Neurobiol* **203**, 102075 (2021).
39. Kang, S. S. *et al.* Identification of plexin A4 as a novel clusterin receptor links two Alzheimer's disease risk genes. *Hum Mol Genet* **25**, 3467–3475 (2016).
40. Kang, S. *et al.* Semaphorin 6D reverse signaling controls macrophage lipid metabolism and anti-inflammatory polarization. *Nat Immunol* **19**, 561–570 (2018).
41. Ulland, T. K. & Colonna, M. TREM2 — a key player in microglial biology and Alzheimer disease. *Nat Rev Neurol* **14**, 667–675 (2018).
42. Atagi, Y. *et al.* Apolipoprotein E Is a Ligand for Triggering Receptor Expressed on Myeloid Cells 2 (TREM2). *J Biol Chem* **290**, 26043–26050 (2015).
43. Yeh, F. L., Wang, Y., Tom, I., Gonzalez, L. C. & Sheng, M. TREM2 Binds to Apolipoproteins, Including APOE and CLU/APOJ, and Thereby Facilitates Uptake of Amyloid-Beta by Microglia. *Neuron* **91**, 328–340 (2016).
44. Neuner, S. M., Tcw, J. & Goate, A. M. Genetic architecture of Alzheimer's disease. *Neurobiol Dis* **143**, 104976 (2020).
45. Rogaeva, E. *et al.* The neuronal sortilin-related receptor SORL1 is genetically associated with Alzheimer disease. *Nat Genet* **39**, 168–177 (2007).
46. Yin, R.-H., Yu, J.-T. & Tan, L. The Role of SORL1 in Alzheimer's Disease. *Mol Neurobiol* **51**, 909–918 (2015).
47. Deming, Y. *et al.* The MS4A gene cluster is a key modulator of soluble TREM2 and Alzheimer's disease risk. *Sci Transl Med* **11**, eaau2291 (2019).
48. Chen, S. *et al.* Spatially resolved transcriptomics reveals genes associated with the vulnerability of middle temporal gyrus in Alzheimer's disease. *Acta Neuropathol Commun* **10**, 188 (2022).
49. Keren-Shaul, H. *et al.* A Unique Microglia Type Associated with Restricting Development of Alzheimer's Disease. *Cell* **169**, 1276-1290.e17 (2017).
50. McQuade, A. *et al.* Development and validation of a simplified method to generate human microglia from pluripotent stem cells. *Mol Neurodegener* **13**, 67 (2018).
51. Wang, W.-Y., Tan, M.-S., Yu, J.-T. & Tan, L. Role of pro-inflammatory cytokines released from microglia in Alzheimer's disease. *Ann Transl Med* **3**, 136 (2015).
52. Grubman, A. *et al.* Transcriptional signature in microglia associated with Aβ plaque phagocytosis. *Nat Commun* **12**, 3015 (2021).
53. Safaiyan, S. *et al.* White matter aging drives microglial diversity. *Neuron* **109**, 1100-1117.e10 (2021).
54. Jay, T. R., von Saucken, V. E. & Landreth, G. E. TREM2 in Neurodegenerative Diseases. *Mol Neurodegener* **12**, 56 (2017).
55. McQuade, A. *et al.* Gene expression and functional deficits underlie TREM2-knockout microglia responses in human models of Alzheimer's disease. *Nat Commun* **11**, 5370 (2020).
56. Takegahara, N. *et al.* Plexin-A1 and its interaction with DAP12 in immune responses and bone homeostasis. *Nature Cell Biology* **8**, 615–22 (2006).
57. Kumanogoh, A. & Kikutani, H. Immunological functions of the neuropilins and plexins as receptors for semaphorins. *Nature Reviews. Immunology* **13**, 802–14 (2013).
58. Han, Q. *et al.* Common Variants in PLXNA4 and Correlation to CSF-related Phenotypes in Alzheimer's Disease. *Frontiers in Neuroscience* **12**, (2018).
59. Macedo, A. *et al.* Risk Variants in Three Alzheimer's Disease Genes Show Association with EEG Endophenotypes. *J Alzheimers Dis* **80**, 209–223 (2021).

60. Deming, Y. *et al.* Genome-wide association study identifies four novel loci associated with Alzheimer's endophenotypes and disease modifiers. *Acta Neuropathol* **133**, 839–856 (2017).
61. Zettergren, A. *et al.* Association of IL1RAP-related genetic variation with cerebrospinal fluid concentration of Alzheimer-associated tau protein. *Sci Rep* **9**, 2460 (2019).
62. Su, F., Bai, F. & Zhang, Z. Inflammatory Cytokines and Alzheimer's Disease: A Review from the Perspective of Genetic Polymorphisms. *Neurosci Bull* **32**, 469–480 (2016).
63. Ogunmokun, G. *et al.* The Potential Role of Cytokines and Growth Factors in the Pathogenesis of Alzheimer's Disease. *Cells* **10**, 2790 (2021).
64. Mendiola, A. S. & Cardona, A. E. The IL-1β phenomena in neuroinflammatory diseases. *J Neural Transm (Vienna)* **125**, 781–795 (2018).
65. Mathys, H. *et al.* Single-cell transcriptomic analysis of Alzheimer's disease. *Nature* **570**, 332–337 (2019).
66. Stuart, T. *et al.* Comprehensive Integration of Single-Cell Data. *Cell* **177**, 1888-1902.e21 (2019).
67. Del-Aguila, J. L. *et al.* A single-nuclei RNA sequencing study of Mendelian and sporadic AD in the human brain. *Alzheimers Res Ther* **11**, 71 (2019).
68. Hafemeister, C. & Satija, R. Normalization and variance stabilization of single-cell RNA-seq data using regularized negative binomial regression. *Genome Biol* **20**, 296 (2019).
69. Zhang, Y. *et al.* Model-based Analysis of ChIP-Seq (MACS). *Genome Biol* **9**, R137 (2008).
70. Amemiya, H. M., Kundaje, A. & Boyle, A. P. The ENCODE Blacklist: Identification of Problematic Regions of the Genome. *Sci Rep* **9**, 9354 (2019).
71. Pliner, H. A. *et al.* Cicero Predicts cis-Regulatory DNA Interactions from Single-Cell Chromatin Accessibility Data. *Mol. Cell* **71**, 858-871.e8 (2018).
72. Patel, A., Garcia Diaz, A., Moore, J. C., Sirabella, D. & Corneo, B. Establishment and characterization of two iPSC lines derived from healthy controls. *Stem Cell Res* **47**, 101926 (2020).
73. Stine, W. B., Dahlgren, K. N., Krafft, G. A. & LaDu, M. J. In vitro characterization of conditions for amyloid-beta peptide oligomerization and fibrillogenesis. *J Biol Chem* **278**, 11612–11622 (2003).
74. Kim, D., Paggi, J. M., Park, C., Bennett, C. & Salzberg, S. L. Graph-based genome alignment and genotyping with HISAT2 and HISAT-genotype. *Nat Biotechnol* **37**, 907–915 (2019).
75. Love, M. I., Huber, W. & Anders, S. Moderated estimation of fold change and dispersion for RNA-seq data with DESeq2. *Genome Biol* **15**, 550 (2014).
76. Benjamini, Y. & Hochberg, Y. Controlling the False Discovery Rate: A Practical and Powerful Approach to Multiple Testing. *Journal of the Royal Statistical Society: Series B (Methodological)* **57**, 289–300 (1995).
77. Szklarczyk, D. *et al.* The STRING database in 2021: customizable protein-protein networks, and functional characterization of user-uploaded gene/measurement sets. *Nucleic Acids Res* **49**, D605–D612 (2021).
78. Shannon, P. *et al.* Cytoscape: a software environment for integrated models of biomolecular interaction networks. *Genome Res* **13**, 2498–2504 (2003).
79. Morris, J. H. *et al.* clusterMaker: a multi-algorithm clustering plugin for Cytoscape. *BMC Bioinformatics* **12**, 436 (2011).
80. Shannon, C. E. A Mathematical Theory of Communication. *Bell System Technical Journal* **27**, 379–423 (1948).
81. Margolin, A. A. *et al.* ARACNE: an algorithm for the reconstruction of gene regulatory networks in a mammalian cellular context. *BMC Bioinformatics* **7 Suppl 1**, S7 (2006).
82. Langfelder, P. & Horvath, S. WGCNA: an R package for weighted correlation network analysis. *BMC Bioinformatics* **9**, 559 (2008).

83. He, L. *et al.* NEBULA is a fast negative binomial mixed model for differential or co-expression analysis of large-scale multi-subject single-cell data. *Commun Biol* **4**, 629 (2021).
84. Kleshchevnikov, V. *et al.* Cell2location maps fine-grained cell types in spatial transcriptomics. *Nat Biotechnol* **40**, 661–671 (2022).

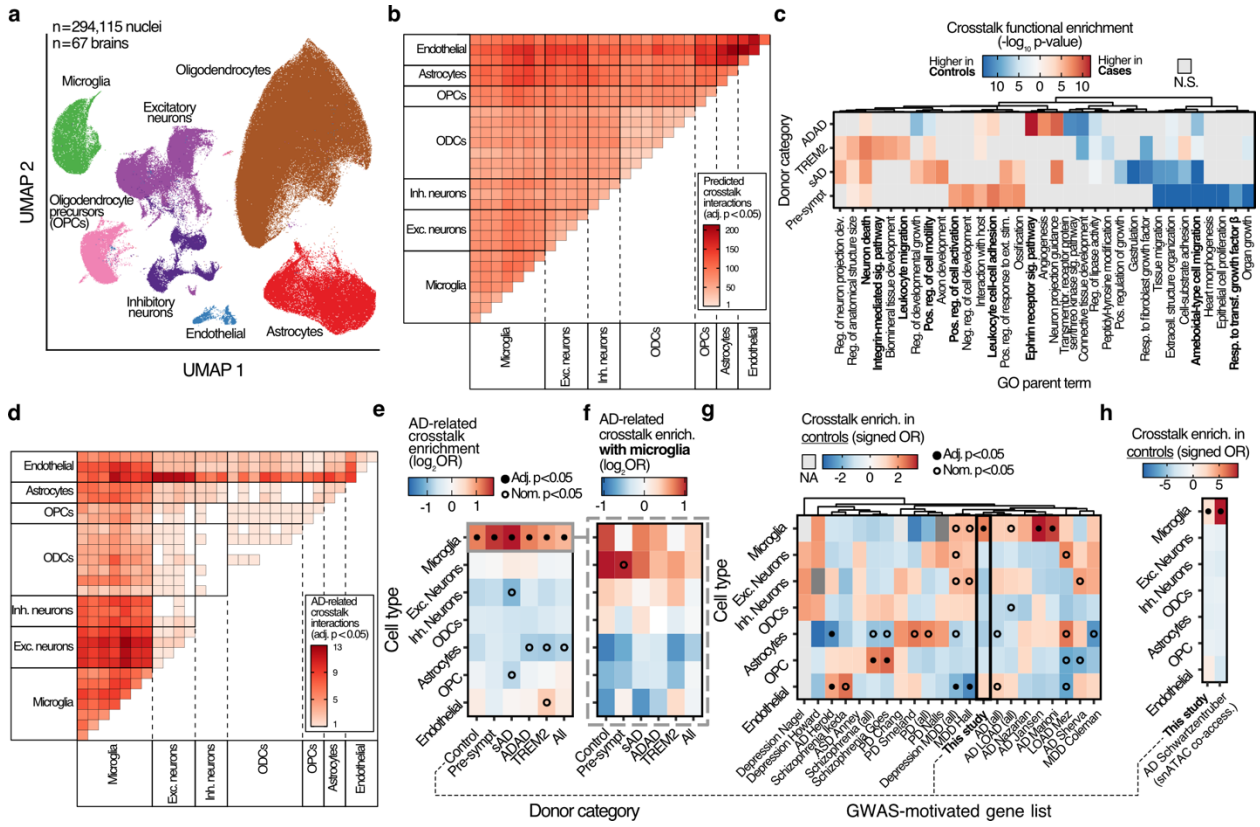

Figure 1: Overview of predicted cellular crosstalk interactions in human brains. a) Uniform Manifold Approximation and Projection (UMAP) representation of the snRNA-seq dataset identifying the seven major brain cell types investigated in this study. **b)** Number of unique significant CellPhoneDB interactions detected involving each cell type as either the ligand or receptor across donor categories. **c)** Gene ontology enrichments of crosstalk interactions up- or down-regulated between each donor category versus controls. **d)** Cellular crosstalk interactions involving one AD gene as either ligand or receptor across all cellular state pairs. **e)** Enrichment of AD crosstalk interactions involving each cell type in each donor category. **f)** Enrichment of AD crosstalk interactions between microglia and other cell types (labeled in the y-axis). **g)** Crosstalk enrichments for each cell type (control donors only) in genes nominated by GWAS from other neuropsychiatric traits. **h)** Similar to (g) but using only AD genes supported by snATAC-seq co-accessibility (Methods). Odds ratios in (e-h) were calculated using Fisher exact tests (Methods).

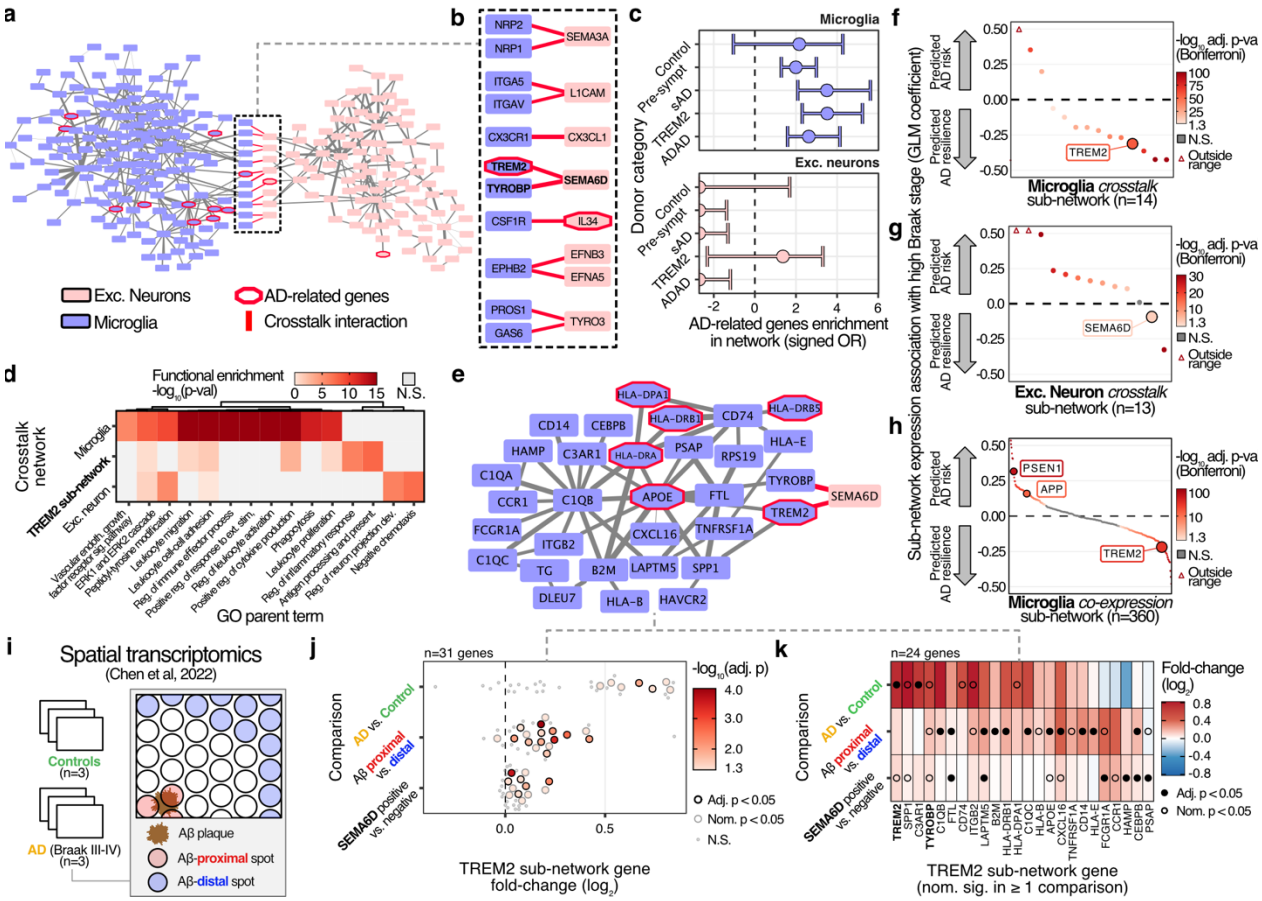

Figure 2: Crosstalk interactions between neurons and microglia are predicted to modulate AD risk genes. a) Microglia-excitatory neuron crosstalk network inferred by CytoTalk. **b)** Prioritized crosstalk interactions using CytoTalk. **c)** Enrichment of AD genes in the microglia crosstalk network across donor categories. **d**) GO enrichments for the genes participating in microglia and excitatory neurons crosstalk networks. **e)** Predicted TREM2 crosstalk subnetwork **f)** Association of microglia crosstalk subnetworks with high Braak stages. **g)** Association of all microglia subnetworks with Braak stages. **h)** Association excitatory neuron crosstalk subnetworks with high Braak stage. **i)** Spatial transcriptomics validation cohort overview. **j)** Changes in gene expression in the *TREM2* crosstalk sub-network associated with disease status, Aβ plaque proximity, and presence of *SEMA6D*-expressing cells. **k)** Individual gene view for comparisons in (j). GLM: generalized linear model.

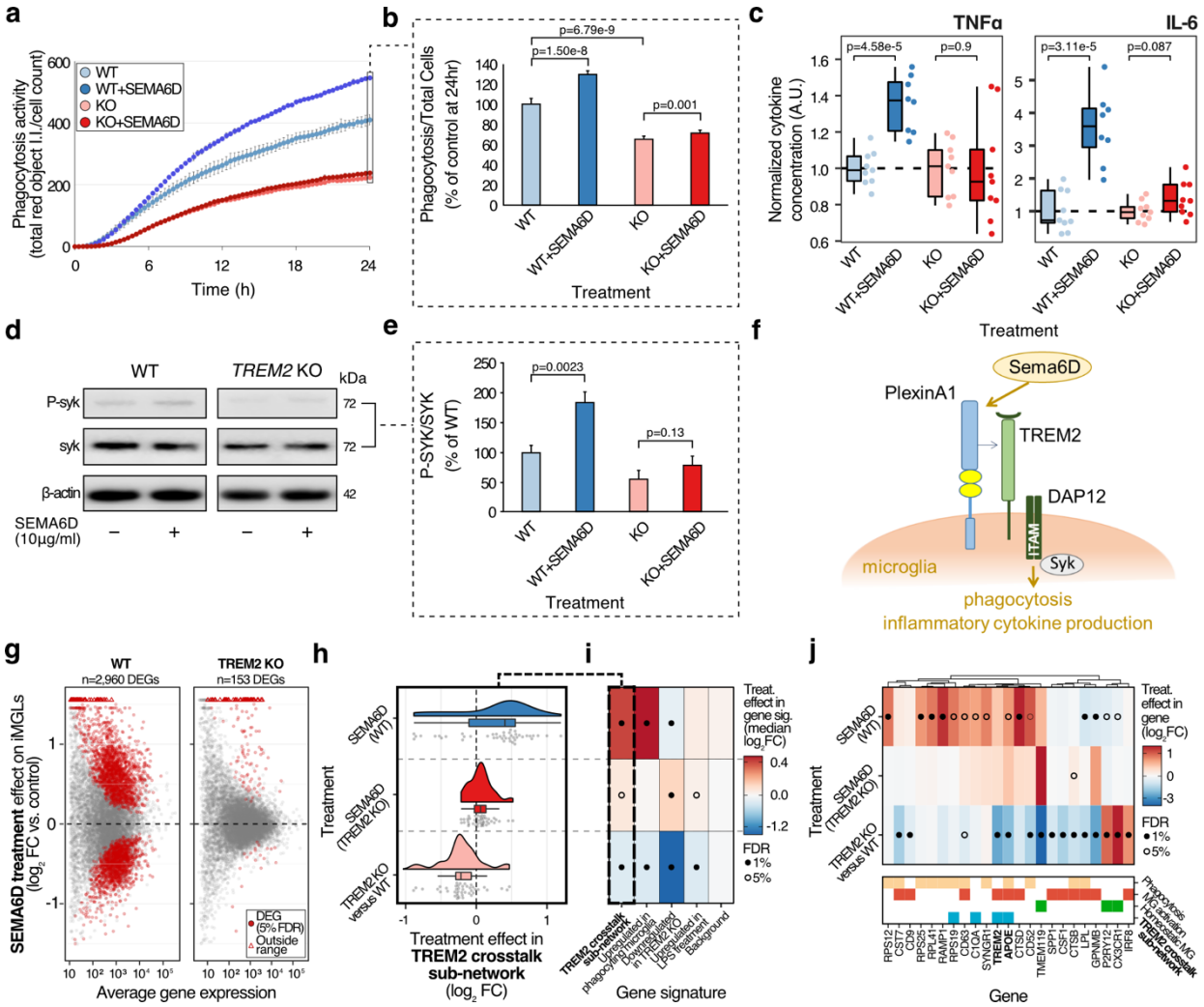

Figure 3. SEMA6D treatment induces microglia activation in a TREM2-dependent manner. **a)** Phagocytosis of synaptosomes by WT or *TREM2* KO iMGL treated with SEMA6D (5 µg/ml). I.I., integrated intensity. Data averaged from three independent experiments (shown in Supp. Figure 11); mean ± SD values. **b)** Quantification of phagocytosis of synaptosomes by WT or *TREM2* KO iMGL treated with SEMA6D at 24 hr. Data represent three independent experiments performed in triplicate; mean ± SEM values at 24 hrs, *p*-values obtained from meta-analyzing the three experiments. **c)** Quantification of media from WT or *TREM2* KO iMGL treated with SEMA6D (10 µg/ml) for cytokine release of TNF-α and IL-6, using the Mesoscale V-plex neuroinflammation panel. Boxplots indicate median and interquartile ranges, *p*-values calculated using linear regression. **d)** Representative western blot analysis of p-SYK and total SYK in WT and *TREM2* KO iMGL treated with SEMA6D (10 µg/ml). β-actin as loading control **e)** Quantification of p-SYK/total SYK western blot analysis, n=3 (d). **f)** Schematic of the proposed SEMA6D-TREM2/DAP12 signaling complex. **g)** RNA-seq effect size distribution on SEMA6D-treated iMGL (WT and *TREM2* KO). **h)** Transcriptional changes in the *TREM2* crosstalk sub-network associated with SEMA6D treatment (WT or *TREM2* KO vs. untreated control) or *TREM2* KO (*TREM2* KO vs. WT, no treatment). Only *TREM2* sub-network genes differentially expressed in at least one comparison were included. **i)** Transcriptional effects of the same conditions as (b) across biologically relevant gene signatures. Background corresponds to 500 randomly selected genes. Solid dots correspond to a 1% FDR significance threshold for comparing the effect size distribution to the corresponding background (Mann-Whitney test). **j)**

Transcriptional effects of the experimental conditions across a representative subset of highly differentially expressed genes from the signatures in (i).